Circuit-specific alterations of *N*-methyl-D-aspartate receptor subunit 1 in the dentate gyrus of aged monkeys

(glutamate receptors/hippocampus)

A. H. Gazzaley*, S. J. Siegel*, J. H. Kordower†, E. J. Mufson†, and J. H. Morrison*‡

*Fishberg Research Center for Neurobiology and Department of Geriatrics and Adult Development, Mount Sinai School of Medicine, New York, NY 10029; and †Department of Neurological Sciences, Rush Presbyterian-St. Luke's Medical Center, Chicago, IL 60612

ABSTRACT Age-associated memory impairment occurs frequently in primates. Based on the established importance of both the perforant path and *N*-methyl-D-aspartate (NMDA) receptors in memory formation, we investigated the glutamate receptor distribution and immunofluorescence intensity within the dentate gyrus of juvenile, adult, and aged macaque monkeys with the combined use of subunit-specific antibodies and quantitative confocal laser scanning microscopy. Here we demonstrate that aged monkeys, compared to adult monkeys, exhibit a 30.6% decrease in the ratio of NMDA receptor subunit 1 (NMDAR1) immunofluorescence intensity within the distal dendrites of the dentate gyrus granule cells, which receive the perforant path input from the entorhinal cortex, relative to the proximal dendrites, which receive an intrinsic excitatory input from the dentate hilus. The intradendritic alteration in NMDAR1 immunofluorescence occurs without a similar alteration of non-NMDA receptor subunits. Further analyses using synaptophysin as a reflection of total synaptic density and microtubule-associated protein 2 as a dendritic structural marker demonstrated no significant difference in staining intensity or area across the molecular layer in aged animals compared to the younger animals. These findings suggest that, in aged monkeys, a circuit-specific alteration in the intradendritic concentration of NMDAR1 occurs without concomitant gross structural changes in dendritic morphology or a significant change in the total synaptic density across the molecular layer. This alteration in the NMDA receptor-mediated input to the hippocampus from the entorhinal cortex may represent a molecular/cellular substrate for age-associated memory impairments.

Memory loss is a consistent feature of Alzheimer disease (AD) and has been linked to severe structural alterations in the perforant path (1–3), an excitatory projection of the entorhinal cortex to the hippocampal dentate gyrus (4). Both human (5) and nonhuman primates (6) also frequently experience age-related memory loss in the absence of overt AD symptoms. However, while certain pathological profiles seen in AD (e.g., amyloid plaques) are present in normal primate aging (7), similar dramatic structural deterioration of the perforant path does not seem to occur (3, 8, 9). This suggests that rather subtle molecular changes in structurally intact neural circuits crucial for memory processes may mediate age-associated memory impairment. The important role of both the perforant path and *N*-methyl-D-aspartate (NMDA) receptors in memory processing (10, 11) and long-term potentiation (LTP) (12, 13), a cellular model for learning, has been extensively documented. Recently, the NMDA receptor distribution within the adult primate hippocampus, has been investigated by immunohistochemical methods (14) and has confirmed both autoradio-graphic (15) and physiological (4) results, which reveal a significant NMDA receptor presence at the perforant path termination zone in the outer molecular layer (OML) of the dentate gyrus. However, there is no information available as to the integrity of the NMDA receptor complex within the dentate gyrus of the aged primate. This is investigated in the present study by using a monoclonal antibody specific to NMDA receptor subunit 1 (NMDAR1) (14). NMDAR1 is an obligatory subunit of the NMDA receptor complex and was therefore used as a marker of all NMDA receptors (16).

Autoradiographic ligand binding studies have suggested that NMDA receptors, as well as non-NMDA glutamate receptors (GluRs), are affected by the normal aging process (17, 18). However, many such analyses were performed on rodents, which differ from primates in certain elements of hippocampal circuitry (19) and possibly in their anatomical alterations associated with aging (8, 9, 20, 21). Furthermore, autoradiographic ligand binding techniques lack dendritic resolution and receptor subunit specificity, which precludes the identification and localization of subcellular subunit changes, as well as the determination of the degree to which receptor alterations are accompanied by structural degeneration. In this study, we used confocal laser scanning microscopy (CLSM) to clearly resolve individual immunofluorescent dendrites and quantitative techniques with a broad array of immunohistochemical probes to determine whether receptor changes are due to alterations in receptor concentration within the dendrites or are the result of dendritic structural reorganization.

In addition to NMDA GluRs, there is growing evidence of the involvement of non-NMDA GluRs in learning and memory-associated processes such as LTP (22). Non-NMDA GluRs have also been demonstrated by immunocytochemical techniques to be present postsynaptically in the OML of the dentate gyrus (23). To investigate the possibility of concurrent changes in these receptors, quantitative CLSM was performed on tissue immunolabeled with antibodies to both AMPA receptor subunits 2/3 (GluR2/3) (24), and kainate receptor subunits 5/6/7 (GluR5/6/7) (25).

MATERIALS AND METHODS

Animals and Tissue Processing. Eighteen monkeys, consisting of one male and two female juvenile rhesus monkeys (1–2 years old) (*Macaca mulatta*), one adult female and three male rhesus monkeys, five adult male cynomolgus monkeys (5–9 years old) (*Macaca fascicularis*) and six aged female rhesus monkeys (24–32 years old), were used in this study. All

Abbreviations: NMDA, *N*-methyl-D-aspartate; NMDAR1, *N*-methyl-D-aspartate receptor subunit 1; GluR, glutamate receptor; CLSM, confocal laser scanning microscopy; IML, inner molecular layer; OML, outer molecular layer; AD, Alzheimer disease.
‡To whom reprint requests should be addressed at: Box 1065, Fishberg Research Center for Neurobiology, Mount Sinai School of Medicine, One Gustave L. Levy Place, New York, NY 10029.

monkeys received care and treatment in accordance with institutional and NIH guidelines. The animals used in the quantitative analysis were raised in captivity and housed in single cages for most of their lives. All aged monkeys used in this study were retired breeders and were not involved previously in any pharmacological or invasive studies. Monthly serological tests, annual physical exams, and necroscopy analyses failed to discern any age-related changes that covaried with the findings obtained in this study. The aged monkeys could not be behaviorally tested due to age-related physical impairments such as cataracts and arthritis which make testing difficult but are unlikely to directly impact on hippocampal GluRs. The animals were deeply anesthetized with ketamine hydrochloride (25 mg/kg, i.m.) and sodium pentobarbital (Nembutal) (30 mg/kg, i.v.) and perfused transcardially with ice-cold 1% paraformaldehyde in 0.1 M phosphate-buffered saline (PBS) for 1 min, followed by 10–14 min of ice-cold 4% paraformaldehyde in PBS (0.125% glutaraldehyde was added to the perfusate for the cynomolgus monkeys). The brains were immediately removed, cut into 5-mm blocks in a coronal plane, and postfixed in cold 4% paraformaldehyde in PBS for 6 h. The blocks were cut on a vibratome at a setting of 50 μm.

Immunocytochemistry. Four closely associated but nonadjacent hippocampal sections, at the level of the lateral geniculate nucleus, were incubated with each of the five primary antibodies used in this study at the appropriate dilutions in PBS with 0.5 mg of bovine serum albumin per ml for 48 h. Only sections incubated in the primary antibody for microtubule-associated protein 2 (MAP2) contained 0.3% Triton X-100. Sections were then washed three times in PBS, transferred to biotinylated anti-mouse IgG heavy and light chain (except for sections treated with primary antibody to GluR 2/3 which were transferred to biotinylated anti-rabbit IgG) for 2 h, washed again in PBS, and transferred to fluorescein isothiocyanate (FITC)-conjugated Avidin for 1 h. Sections were then mounted and coverslipped with Vectashield (Vector Laboratories) to reduce fluorescence quenching.

CLSM and Quantitative Evaluation. Quantitative CLSM analysis was performed on the most recently perfused rhesus monkeys of the three age groups to ensure a comparably high quality of immunocytochemical staining essential for this analysis (juvenile, $n = 3$; adult, $n = 3$; aged, $n = 4$). Two sections from each animal were selected for analysis with a Zeiss LSM 410 inverted confocal microscope. On all sections analyzed, FITC was excited by an argon/krypton laser at 488 nm that was attenuated by a 90% neutral density filter, reflected to the specimen with an FT488/568 dichroic mirror, and imaged with a Zeiss Plan-Neofluar $\times$63/1.25 numerical aperture oil immersion objective. A confocal aperture was set with a digital pinhole size of 17. A suitable contrast/brightness setting that yielded a high-resolution image for both bright and dim sections, without regions above the maximal pixel intensity of 255, was determined for each antibody.

To control for inherent bias, the area in each section where the lamination effect was maximally observed was selected for quantitative sampling in every animal from all three age groups. For each section, six fields within the inner molecular layer (IML) (dendritic field immediately distal to the granule cell layer) and OML (midpoint between the granule cell layer border and the hippocampal fissure) were randomly chosen in the selected area. Thus, 24 fields were sampled from each animal for each antibody used in the quantitative analysis. Each field was scanned one time at a predetermined z-axis distance into the tissue with a two-line average for a total scan time of 4.52 s and an electronic zoom factor of 4.5 (which increases the resolution to 0.0881 μm/pixel, resulting in scanned regions of identical area (2039 μm^2). Each digitized image consisted of a 512 $\times$ 512 $\times$ 8-bit pixel array in which every pixel was assigned a gray level intensity value ranging from 0 to 255. Subtraction of background immunofluorescence

was accomplished with a photometric offset (Zeiss) to establish a pixel intensity threshold below which a pixel would have no contribution to the average pixel intensity or area of the field. The offset was accomplished by viewing the image at a display magnification of $\times$2 and increasing the thresholding value until the blue-colored display, designating the thresholded area, abutted the dendrites (Fig. 1). The average pixel intensity and area of the portion of the field above threshold were calculated, thus representing the immunofluorescence intensity and area of the granule cell dendritic shafts only.

The OML/IML ratio of the intensity and area measurements were then computed for each animal by dividing the mean of the 12 OML values by the mean of the 12 IML values. The mean ratio value for each age group was then obtained from these individual ratios. The OML/IML ratio was used, as opposed to absolute comparisons, to control for any methodological variability in staining intensity that existed between the sections.

RESULTS

NMDAR1 Immunofluorescence. In juvenile and adult monkeys, NMDAR1 immunofluorescence was present within the pyramidal cell bodies and throughout the dendritic arbor of the subiculum and all fields of Ammon's horn, as described (14). The receptor distribution and intensity within these regions, as well as within both temporal and prefrontal neocortical areas, were indistinguishable from that observed in the aged monkeys, based on nonquantitative microscopic analysis. A similar examination of the dentate gyrus of juvenile and adult monkeys revealed somatic granule cell labeling with a relatively homogeneous distribution of immunofluorescence throughout the dendritic extent of the molecular layer (Fig. 2 *A–C*). In contrast, the molecular layer of all the aged monkeys in this study exhibited a striking reduction in the immunofluorescence intensity in the OML compared to the IML (Fig. 2 *D–F*). By visual inspection, certain areas of the dentate gyrus, within a given section, exhibited this lamination pattern to a greater degree than other areas. However, this partial heterogeneity in the pattern had no consistent regional distribution in the dentate gyrus.

Quantitative CLSM analysis of the areas of maximal lamination, revealed that the OML/IML dendritic intensity ratios of the juvenile and adult monkeys were not significantly different from each other but were significantly different from those of the aged monkeys (34.4% and 30.6%, respectively), which exhibited a markedly lower intensity of immunofluo-
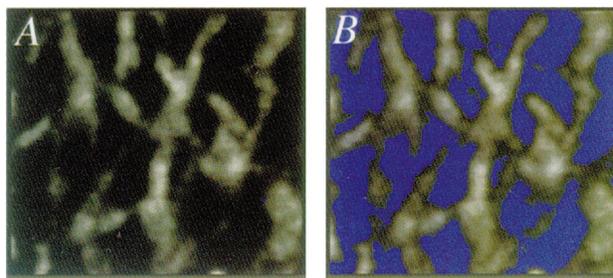

Fig. 1.   CLSM image of NMDAR1-immunolabeled granule cell dendrites without (*A*) and with (*B*) intensity thresholding denoted by a blue-color overlay. The intensity thresholding effectively removes all nondendritic portions of the field from entering into average measurements of fluorescence intensity or area. In this example, thresholding corrects the average gray level intensity of the field (*A*, 26.9) to obtain a more accurate reflection of the immunofluorescence intensity within the granule cell dendrites (*B*, 37.6). By this same process, the area of the field prior to thresholding (*A*, 148 μm^2) was corrected to determine the immunofluorescent dendritic area within the field (*B*, 99 μm^2). The areas of the individual fields quantified in this study were $\approx$14-fold larger than shown here (i.e., 2039 μm^2).
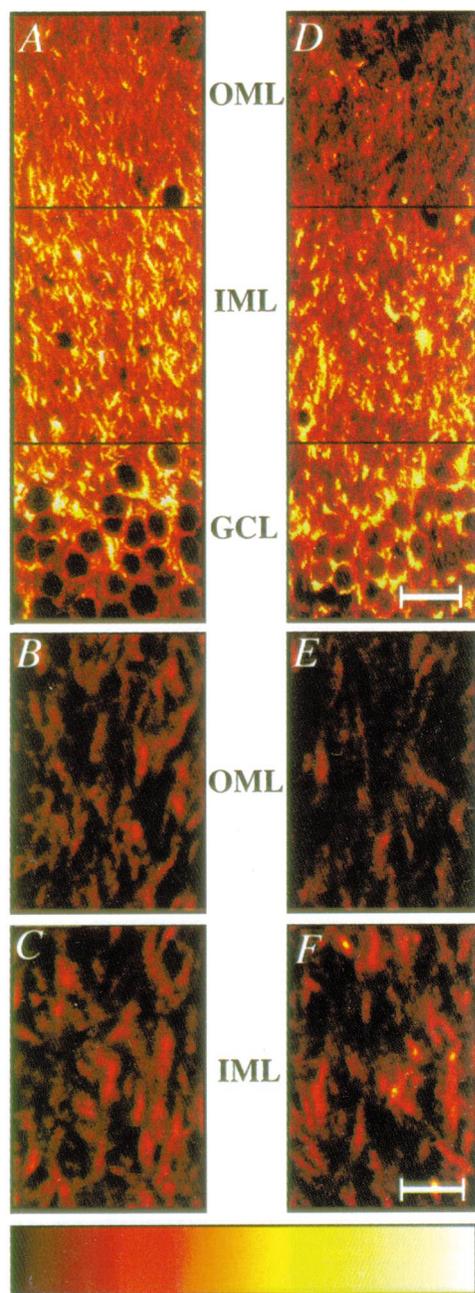
FIG. 2. Localization of NMDAR1 immunofluorescence in the dentate gyrus, displayed as glow-scale pseudocolored CLSM images. Glow-scale pseudocoloring mimics the heat scale and is a frequently used means of viewing differences in intensity levels. The lower intensity dendritic segments are orange-red and the higher intensity dendritic segments are yellow-white. The glow-scale bar demonstrates the color gradient of this scale. (*A–C*) CLSM images from an adult rhesus monkey (5–9 years old). (*A*) Low-power image revealing a relatively homogeneous pattern of immunofluorescence labeling throughout the molecular layer, with most of the field in the IML and OML consisting of low intensity (orange-red) dendritic segments. (*B* and *C*) At higher magnification, a similar, although slightly lower, intensity of labeling is apparent within the OML dendrites (*B*) compared to the IML dendrites (*C*). (*D*) NMDAR1 immunolabeling in an aged rhesus monkey (32 years old), demonstrating a pronounced decrease in the immunofluorescence intensity within the dendritic field of the OML compared to the IML, as visualized by the darker red dendritic segments in the OML. (*E* and *F*) At higher magnification, a markedly reduced labeling intensity is visible within individual dendritic segments of the OML (*E*) relative to the IML (*F*). GCL, granule cell layer. (Bars: *A* and *D*, 25 μm; *B, C, E*, and *F*, 10 μm.)

rescence within the dendritic segments of the OML compared to the IML (Table 1). This decrease in the OML/IML intensity ratio was observed in all of the aged monkeys in this study.

Non-NMDA Receptor Immunofluorescence. In contrast to the NMDAR1 result, we observed a relatively homogeneous staining intensity, with antibodies to GluR5/6/7 and GluR2/3, throughout the molecular layer in animals of all age groups (Fig. 3 *A–D*), comparable to the recent observation of uniform molecular layer labeling with an antibody to GluR2/3 in aged humans (26). Quantitative analysis demonstrated no statistically significant difference between the aged and adult monkeys for either antibody (Table 1). This suggests that the intradendritic change in GluR concentration from adulthood to old age was NMDA receptor specific, although a larger sample size may have revealed subtle shifts in non-NMDA GluRs. A small, but statistically significant difference between the juveniles and adults for GluR5/6/7 labeling (Table 1) was also observed. This may represent a developmental shift in the kainate subunit pattern, comparable to morphological alterations that occur during development of the primate granule cell dendrites (27).

Dendritic Area. In addition to determining the immunofluorescence intensity, we investigated whether there was a loss of dendritic area in the OML relative to the IML in aged monkeys (Fig. 1). Analyses of the adult and aged animals demonstrated no significant difference in immunofluorescent dendritic area across the molecular layer for any of the GluR subtypes examined (Table 1). To explore further the possibility of structural alterations, we immunolabeled hippocampal sections with a monoclonal antibody to the soma/dendrite-specific cytoskeletal protein MAP2 (28). Qualitative (Fig. 3 *E* and *F*) and quantitative examination revealed no significant age-associated differences in either dendritic immunofluorescence intensity or area across the molecular layer (Table 1).

Synaptic Density. To investigate whether the NMDAR1 alteration was associated with a change in synaptic density across the laminae of the dentate gyrus, hippocampal sections were incubated with a monoclonal antibody to synaptophysin (29) (Fig. 3 *G* and *H*), an integral membrane glycoprotein of synaptic vesicles that has been used extensively as a reflection of total synaptic density (30). Quantitative analyses determined that there was no significant age-associated difference in the OML/IML ratio of either the synaptophysin immunofluorescence intensity or area (Table 1), suggesting the preservation of total synaptic density in the OML relative to the IML.

DISCUSSION

In the present study we demonstrated a change in NMDAR1 immunofluorescence intensity at the intradendritic level by using CLSM and gray level intensity quantification. Previous investigations have demonstrated that immunoreactive intensity is a reflection of protein concentration (31), suggesting that our results reveal a relative decrease in the cytoplasmic pool of NMDAR1 within the distal segments of the granule cell dendrites that comprise the perforant path terminal zone (OML). Both immunofluorescence area data for the GluRs and MAP2 suggest that the relative decrease in NMDAR1 concentration within the distal granule cell dendrites occurs without concomitant major dendritic structural alterations, which is in contrast to the severe dendritic pruning of the granule cells that occurs in AD (3). We have also demonstrated by quantitative measures that the receptor change was NMDA receptor specific, even though all three classes of GluRs are colocalized within these dendrites (23). This suggests that the intradendritic parcellation of a neurotransmitter receptor is specifically modifiable in an age-related and circuit-specific manner.

Both entorhinal lesion experiments in animals and postmortem analyses of AD brains have revealed a dramatic decrease

Table 1.   Quantitative CLSM data

Antibody to	Age group	Mean intensity ratio (OML/IML)	% difference	Mean area ratio (OML/IML)	% difference
NMDAR1	Juvenile	0.90 ± 0.05[†] }	-5.6	0.94 ± 0.07 }	-13.8
	Adult	0.85 ± 0.03 }	-30.6***	0.81 ± 0.09 }	$+9.9$
	Aged	0.59 ± 0.01 }		0.89 ± 0.09 }	
GluR2/3	Juvenile	0.90 ± 0.11 }	-10.0	0.96 ± 0.02 }	-2.1
	Adult	0.81 ± 0.04 }	$+2.5$	0.94 ± 0.15 }	$+3.2$
	Aged	0.83 ± 0.08 }		0.97 ± 0.08 }	
GluR5/6/7	Juvenile	0.95 ± 0.06 }	-10.5*	1.05 ± 0.02 }	-10.5**
	Adult	0.85 ± 0.01 }	-2.4	0.94 ± 0.02 }	-5.3
	Aged	0.83 ± 0.05 }		0.89 ± 0.06 }	
MAP2	Juvenile	0.91 ± 0.07 }	$+9.9$	0.99 ± 0.13 }	-6.1
	Adult	1.00 ± 0.10 }	-10.0	0.93 ± 0.03 }	$+1.1$
	Aged	0.90 ± 0.08 }		0.94 ± 0.05 }	
Synaptophysin	Juvenile	1.16 ± 0.13 }	-12.9	1.04 ± 0.13 }	-1.0
	Adult	1.01 ± 0.09 }	0	1.05 ± 0.01 }	$+7.6$
	Aged	1.01 ± 0.04 }		1.13 ± 0.07 }	

   Quantitative CLSM analyses demonstrating percentage difference between age groups in the fluorescence intensity and area of the dendritic segments within the OML/IML for all five antibodies analyzed. Percentage difference refers to the increase ($+$) or decrease ($-$) when comparing the younger group to the older group—i.e., (adult-juvenile)/juvenile, (aged-adult)/adult. Note that the only statistically significant difference in intensity, or area, when comparing adult to aged is the decrease in the fluorescence intensity ratio of the OML/IML for NMDAR1 labeling. In addition, a small but statistically significant percentage decrease is evident for GluR5/6/7 intensity and area ratios when comparing juveniles to adults. Ratios represent means $\pm$ 1 SD.
*$P < 0.05$, **$P < 0.005$, ***$P < 0.0001$ (unpaired Student's *t* test).
[†]The percentage difference from juvenile to aged for NMDAR1 is 34.4% (aged-juvenile/juvenile).

in synaptophysin immunoreactivity within the dentate gyrus OML (2). In this study, however, quantitative analysis revealed no change in the total synaptic density across the molecular layer. In addition, a recent quantitative study demonstrated that there was no loss of total synapses in the OML of the aged primate dentate gyrus (9) or age-related loss of neurons in layer II of the primate entorhinal cortex (8), in sharp contrast to the extensive neuronal loss in this region in AD (1). It should be noted that these reports do not parallel the observed loss of synapses in both the middle molecular layer and the IML of aged rats (32) and physiological findings consistent with a reduction in the number of perforant path axons in aged rats (20). These data may reflect species differences between rodents and primates in the effects of aging on these neural circuits. Nevertheless, it appears unlikely that the receptor alterations we observed in the molecular layer of the aged monkeys result from a degeneration of the perforant path with concomitant deafferentation of the dentate gyrus, although the presence of functional changes in the perforant path that are not reflected anatomically (33) cannot be ruled out as contributing factors to the receptor alterations. In addition, given that all the aged animals in this study were female, age-related changes in estrogen levels cannot be excluded as a potential contributing factor.

   The combined use of subunit-specific GluR antibodies with quantitative CLSM analysis has provided a particularly high level of molecular and anatomical resolution in the present analysis, enabling us to demonstrate NMDAR1 subunit-specific changes in receptor concentration within segments of granule cell dendrites that correspond to the laminar segregation of inputs. Although we have not quantitatively ruled out subtle receptor changes in other hippocampal or neocortical regions, we have established that the segregated inputs to the dentate gyrus are differentially affected by aging. Given the crucial role that both the perforant path and NMDA receptors have in learning and memory, we hypothesize that the present findings provide a molecular/cellular substrate that may contribute to age-associated memory impairment, in contrast to the structural disconnections of hippocampal circuits that are a hallmark of AD pathology (1, 2). It will be of great interest

to test this hypothesis in human and nonhuman primate populations with longitudinal behavioral assessment by cor-
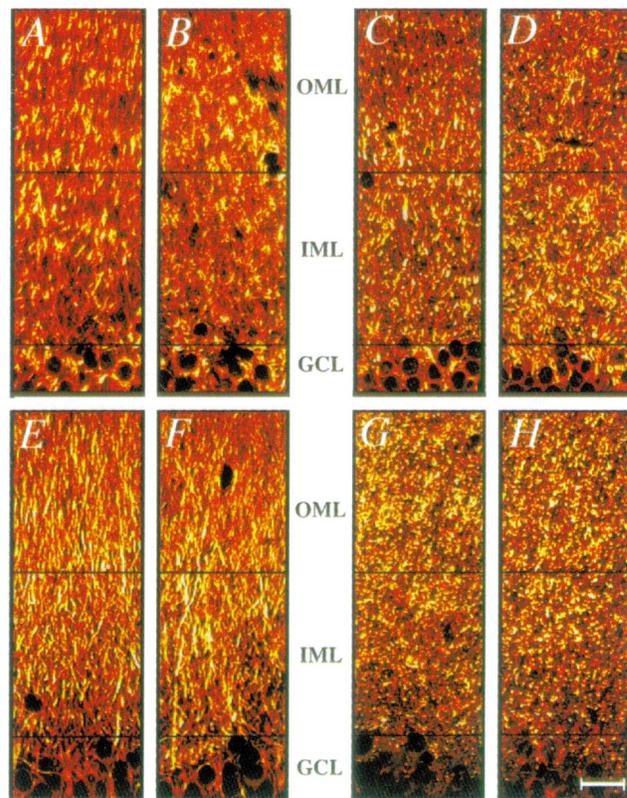

FIG. 3.   Glow-scale pseudocolored CLSM images demonstrating GluR2/3 (*A* and *B*), GluR5/6/7 (*C* and *D*), MAP2 (*E* and *F*), and synaptophysin (*G* and *H*) immunofluorescence in the dentate gyrus of 5- to 9-year-old (*A, C, E,* and *G*) and 25- to 32-year-old (*B, D, F,* and *H*) rhesus monkeys. Note that the fluorescence intensity is fairly uniform throughout the dendritic extent of the molecular layer (OML vs. IML) for all four antibodies in both the adult and aged monkeys. GCL, granule cell layer. (Bars = 25 μm.)

relating subtle circuit-specific molecular changes in the absence of overt neuron and synapse loss with age-related cognitive decline.

1. Hyman, B. T., Van Hoesen, G. W., Damasio, A. R. & Barnes, C. L. (1984) *Science* **225,** 1168–1170.
2. Cabalka, L. M., Hyman, B. T., Goodlett, C. R., Ritchie, T. C. & Van Huesen, G. W. (1992) *Neurobiol. Aging* **13,** 283–291.
3. Flood, D. G., Buell, S. J., Horwitz, G. J. & Coleman, P. D. (1987) *Brain Res.* **402,** 205–216.
4. Lambert, J. D. C. & Jones, R. S. G. (1990) *J. Neurophysiol.* **64,** 119–132.
5. Poon, L. W. (1985) in *Handbook of the Psychology of Aging*, eds. Birren, J. E. & Shaie, K. W. (Van Nostrand Reinhold, New York), pp. 427–462.
6. Rapp, P. R. & Amaral, D. G. (1991) *Neurobiol. Aging* **12,** 481–486.
7. Mufson, E. J., Benzing, W. C., Cole, G. M., Wang, H., Emrich, D. F., Sladek, J. R., Jr., Morrsion, J. H. & Kordower, J. H. (1994) *Neurobiol. Aging* **15,** 621–627.
8. West, M. J., Amaral, D. J. & Rapp, P. R. (1993) *Soc. Neurosci. Abstr.* **19,** 599.
9. Tigges, J., Herndon, J. G. & Rosene, D. L. (1995) *Acta Anat.* **153,** 39–48.
10. Meunier, M., Bachevalier, J., Mishkin, M. & Murray, E. A. (1993) *J. Neurosci.* **13,** 5418–5432.
11. Morris, R. G. M., Anderson, E., Lynch, G. S. & Baudry, M. (1986) *Nature (London)* **319,** 774–776.
12. Bliss, T. V. P. & Lømo, T. (1973) *J. Physiol. (London)* **232,** 331–356.
13. Bliss, T. V. P. & Collingridge, G. L. (1993) *Nature (London)* **361,** 31–39.
14. Siegel, S. J., Janssen, W. G., Gasic, G. P., Jahn, R., Heinemann, S. F. & Morrison, J. H. (1994) *Proc. Natl. Acad. Sci. USA* **91,** 564–568.
15. Cotman, C. W., Monaghan, D. T., Ottersen, O. P. & Storm-Mathisen, J. (1987) *Trends Neurosci.* **10,** 273–280.
16. Monyer, H., Sprengel, R., Shoepfer, R., Herb, A., Higuchi, M., Lomeli, H., Burnashev, N., Sakmann, B. & Seeburg, P. H. (1992) *Science* **256,** 1271–1221.
17. Magnusson, K. R. & Cotman, C. W. (1993) *Neurobiol. Aging* **14,** 197–206.
18. Nicoletti, V. G., Condorelli, D. F., Dell'Albani, P., Ragusa, N. & Giuffrida Stella, A. M. (1995) *J. Neurosci. Res.* **40,** 220–224.
19. Witter, M. P. & Amaral, D. G. (1991) *J. Comp. Neurol.* **307,** 437–459.
20. Barnes, C. A. & McNaughton, B. L. (1980) *J. Physiol. (London)* **309,** 473–485.
21. Geinisman, Y., Morrell, F. & de Toledo-Morrell, L. (1987) *Brain Res.* **423,** 179–188.
22. Maren, S., Georges, T., Standley, S., Baudry, M. & Thompson, R. (1993) *Proc. Natl. Acad. Sci. USA* **90,** 9654–9658.
23. Siegel, S. J., Janssen, W. G., Tullai, J. W., Rogers, S. W., Moran, T., Heinemann, S. F. & Morrison, J. H. (1995) *J. Neurosci.* **15,** 2707–2719.
24. Wenthold, R. J., Yokatani, N., Doi, K. & Wada, K. (1992) *J. Biol. Chem.* **267,** 501–507.
25. Huntley, G. W., Rogers, S. W., Moran, T., Janssen, W., Archin, N., Vickers, J. C., Cauley, K., Heinemann, S. F. & Morrison, J. H. (1993) *J. Neurosci.* **13,** 2965–2981.
26. Hyman, B. T., Penney, J. D. J., Blackstone, C. B. & Young, A. B. (1994) *Ann. Neurol.* **35,** 31–37.
27. Duffy, C. J. & Rakic, P. (1983) *J. Comp. Neurol.* **214,** 224–237.
28. Huber, G. & Matus, A. (1984) *J. Neurosci.* **4,** 151–160.
29. Wiedenmann, B. & Franke, W. W. (1985) *Cell* **41,** 1017–1028.
30. Masliah, E., Mallory, M., Hansen, L., DeTeresa, R. & Terry, R. D. (1993) *Neurology* **43,** 192–197.
31. Good, M. J., Hage, W. J., Mummery, C. L., de Latt, S. W. & Boonstra, J. (1992) *J. Histochem. Cytochem.* **40,** 1353–1361.
32. Geinisman, Y., de Toledo-Morrell, L., Morrell, F., Persina, I. S. & Rossi, M. (1992) *Hippocampus* **2,** 437–444.
33. Barnes, C. A. (1994) *Trends Neurosci.* **17,** 13–18.